JACS
JOURNAL OF THE AMERICAN CHEMICAL SOCIETY
Communication
pubs.acs.org/JACS

Observing Extremely Weak Protein−Protein Interactions with Conventional Single-Molecule Fluorescence Microscopy

Janghyun Yoo,[†,‡,§] Tae-Sun Lee,[‡,§] Byungsan Choi,[†,‡,§] Min Ju Shon,[‡,§] and Tae-Young Yoon*[,‡,§]

[†]Department of Physics, Korea Advanced Institute of Science and Technology (KAIST), Daejeon 34141, South Korea
[‡]Center for Nanomedicine, Institute for Basic Science (IBS), Yonsei University, Seoul 30722, South Korea
[§]Yonsei-IBS Institute, Yonsei University, Seoul 30722, South Korea

Supporting Information

ABSTRACT: Extremely weak protein−protein interactions (PPIs), signified by micromolar or even millimolar dissociation constants, are one of the keys to understanding the rapid responses of cellular systems. Although single-molecule methods are particularly useful in determining kinetics of biological processes, their application is largely limited to rather strong interactions because of the diffraction-limited observation volume. In this study, we report a single-molecule method that allows the characterization of PPIs using a prey concentration 4 orders of magnitude lower than the dissociation constant. Instead of increasing the concentration of diffusing molecules, which is inevitably limited by the optical diffraction limit, we employed an increased density of surface bait protein. The low occupancy of the surface baits permitted determination of the kinetics with single-molecule resolution. We used this approach to study a PPI network consisting of Ras and its downstream proteins including full-length Rafs and catalytic subunits of phosphoinositide 3-kinase.

Most biological information, initially encoded in genomic sequences, is physically embodied as protein−protein interactions (PPIs), which are actual interactions driving biological systems. Proteins interacting with nucleic acids usually exhibit a high specificity and affinity as exemplified by the gene editing tools, which are able to find a target sequence among the whole genome with an estimated dissociation constant (K_d) in picomolar ranges.[1,2] On the contrary, cell signaling proteins are known to exploit weak and transient interactions, which give rapid turnover and facilitate adaption of the signaling circuits to changing environments. The K_d values of these PPIs for cell signaling circuits reportedly range from sub-μM to hundreds of μM.[3,4] Physiological concentrations of cell signaling proteins are approximately in the same range (sub-μM to μM), allowing the cell signaling proteins to find their downstream partners with reasonable probabilities.

Single-molecule studies aim to track movements and/or conformational changes of target single molecules.[5] In the case of total internal reflection (TIR) microscopy, conversion of a far-field propagating optical wave into an evanescent wave limits the excitation depth to thicker than ∼100 nm. Thus, the concentration barrier in single-molecule studies, above which the signal-to-noise ratio becomes <1, is around tens of nM (ref 6), limiting the maximum K_d value accessible with single-molecule TIR fluorescence microscopy to ∼100 nM.

There have been various approaches to overcome the concentration barrier.[7] A simple method is to use prolonged observation time. This approach however requires additional instrumentation to correct stage drift, suffers from photobleaching, and is still limited to maximum sub-μM K_d values. Alternatively, the observation volume can be reduced,[8−11] and the zero-mode waveguide is a notable example.[12−14] The zero-mode waveguide however requires formation of optical cavities with a dimension of half wavelength of the visible light, and thus costly electron beam lithography. Recently, it is demonstrated that the concentration barrier can be avoided by separating the immobilized target molecules from yet diffusing molecules using photoactivatable fluorescence tags.[15] However, determination of K_d values in the micromolar or even millimolar range with single-molecule resolution is undemonstrated.

Here, we developed an approach for studying weak protein−protein interactions using a single-molecule TIR microscope. A conventional single-molecule study sparsely immobilizes baits on the surface (typically, one bait per 10 μm^2) so that binding events on these individual surface baits are resolved as diffraction-limited spots in far-field optical imaging. Instead of increasing the prey protein concentration, which was inevitably limited by the concentration barrier, we take an alternative approach that employs a high surface density of the baits (Figure 1). When we use a prey concentration of 4 orders of magnitude lower than K_d, the bait occupancy would be of the same order of 10^{-4}. If there are $\sim 10^5$ baits immobilized in our imaging area ($\sim$3200 μm^2), we expect 10 single-molecule binding events for a given moment (Figure 1a). We note that this condition corresponds to a surface density of tens of baits per μm^2. Counting the occurrence of these binding events with time can be converted into a kinetic rate for binding between the bait and prey (k_{on}) by the following equation:

$$k_{on} = \frac{f_{bind}}{[prey]\sigma_{bait}A}$$

where f_{bind} is the frequency of binding events, [prey] is the concentration of the prey protein (molar concentration), σ_{bait} is the surface density of the bait protein (number per area), and A is the imaging area. We can also precisely measure the duration

Received: September 19, 2016
Published: October 19, 2016

DOI: 10.1021/jacs.6b09542
J. Am. Chem. Soc. 2016, 138, 14238−14241

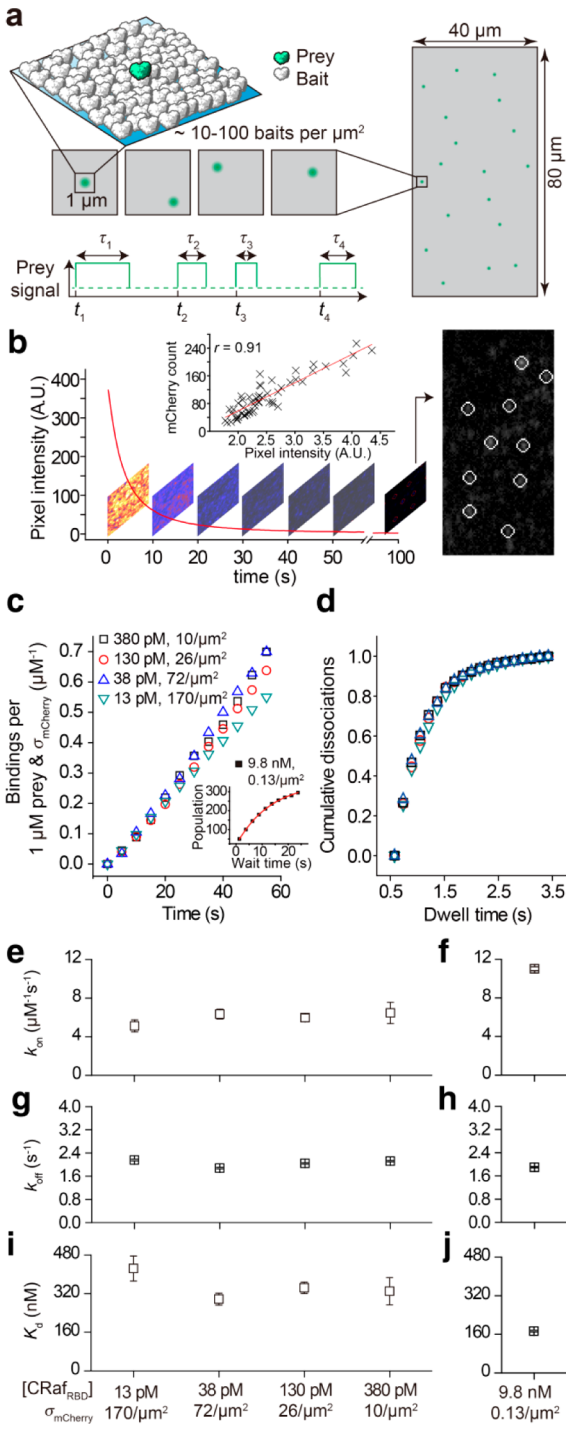

Figure 1. (a) Experimental scheme. The bait density on the surface was increased, typically up to tens of baits per μm^2. In the given imaging area, weak PPIs take place with different baits, which are monitored by single-molecule fluorescence microscopy. (b) Photobleaching analysis for determination of the mCherry-HRas density on surface. Corresponding intensity-to-number relation (inset). (c and d) Cumulative binding events between HRas and $CRaf_{RBD}$ and corresponding dwell time distributions under different reaction conditions. (e) k_{on}, (g) k_{off}, and (i) K_d of the HRas-$CRaf_{RBD}$ interaction. (f) k_{on}, (h) k_{off}, and (j) K_d of the same interaction under a single-bait condition. Error bars are SD for k_{on}, standard errors from exponential regressions for k_{off}, and propagated errors from k_{on} and k_{off} for K_d. The same applies to Figures 2 and 3.

of the individual binding events (Figure 1a). The distributions of the binding duration provide all of the information needed to determine the kinetic rate for dissociation of the bait-prey complexes (k_{off}). A combination of the kinetics rates finally allows determination of the K_d value.

As a precedent PPI, we chose to study the binding between HRas and the Ras-binding domain (RBD) of CRaf.[16,17] We employed single-molecule co-immunoprecipitation (co-IP) analysis.[18−20] We however notice that our approach employing high surface bait densities is not limited to the single-molecule co-IP analysis, but is generally applied to any form of single-molecule studies.

We introduced the Q61L mutation to the HRas gene that makes HRas constitutively active (CA) and fused the gene with a red fluorescent protein, mCherry (Figure SI-1a), which was used throughout this study unless otherwise specified. The $CRaf_{RBD}$ gene was fused with enhanced green fluorescent protein (eGFP) (Figure SI-1b). We expressed mCherry-HRas and eGFP-$CRaf_{RBD}$ in separate groups of HEK293T cells and produced cell lysates, respectively. Using biotinylated anti-mCherry antibodies, the mCherry-HRas proteins were pulled down on a quartz surface coated with polyethylene-glycol (Figure SI-1a). The density of the mCherry-HRas proteins on surface was determined by studying photobleaching of the total mCherry fluorescence intensity integrated over our imaging area. In the tail region of the photobleaching process, where only a few molecules survived in the imaging area, we recorded both the mCherry fluorescence intensity and the number of the survived mCherry-HRas proteins (Figure 1b). This allowed us to generate an intensity-to-number relation (Figure 1b, inset), and with the initial fluorescence intensity value, we estimated the HRas protein density on surface (Figures SI-2−5 and Supplementary Methods).

To initiate PPIs, we introduced eGFP-labeled prey proteins on to the immobilized baits. To record an equilibrium reaction, we started imaging after 30−60 min since injection of the prey proteins. The k_{on} and k_{off} values of the HRas-$CRaf_{RBD}$ binding were determined from the cumulative plots of the binding events and the binding dwell times, respectively (Figures 1c,d and SI-6−12). All the different reaction conditions gave consistent k_{on} and k_{off} values, which were 5.9 ± 0.5 μM^{-1} s^{-1} and 2.0 ± 0.1 s^{-1}, respectively (error values in the main text are SD of all measurements) (Figure 1e,g). These kinetic rates were combined to give a K_d value of around 350 nM (Figure 1i).

The determined k_{off} values were consistent with the previously reported values[16−18] (Figure 1g) and that determined under a typical single-molecule imaging condition (at 0.13 bait per μm^2) (Figures 1h and SI-13; see Supplementary Methods for details of the single-bait imaging). On the contrary, we found that all the k_{on} values determined under high HRas densities were consistently about half of the k_{on} value determined with a single-bait condition (Figure 1e,f). Unlike the single-bait imaging where we included only baits actively interacting with preys, all counted mCherry-labeled HRas proteins were included in our methods using high surface bait densities. Although we could not rule out other physical reasons for this observed difference in k_{on}, we reasoned that only half of the mCherry-labeled HRas proteins on surface were active in binding to $CRaf_{RBD}$ because cell signaling proteins including Ras switch between active and inactive states. The estimated active portion of mCherry-HRas was 54%, which was used for the following analysis in this work.

DOI: 10.1021/jacs.6b09542
J. Am. Chem. Soc. 2016, 138, 14238−14241

Next, we examined the kinetics of the interaction between HRas and full-length Raf proteins. The full-length Rafs are thought to have a weaker interaction with Ras than the truncated RBD domain. We thus used higher concentrations for the prey CRaf protein (0.29−9.6 nM), which were then combined with surface HRas densities ranging from 17.9 to 84.1 per μm^2 (Table SI-1). We first measured the k_{on} kinetic rates, which were largely constant at 0.28 ± 0.05 μM^{-1} s^{-1} in the CRaf concentration range we studied (Figure 2a). The k_{off} values of the HRas-CRaf complex were also maintained at a constant value of 1.0 ± 0.1 s^{-1} (Figures 2b and SI-14).

In similar prey concentration range (0.19−2.61 nM) and surface Ras densities (5.3−172.3 baits per μm^2), we determined the interaction kinetics of HRas and full-length BRaf (Table SI-1). A mutation in the kinase domain of BRaf (V600E) was introduced, which is frequently observed in melanoma and other types of cancers.[21] The k_{on} of the HRas-$BRaf^{V600E}$ complex was very similar to that of the HRas-CRaf complex (Figure 2a, 0.29 ± 0.03 μM^{-1} s^{-1}), but dissociation was slightly slower with a k_{off} of 0.64 ± 0.04 s^{-1} (Figure 2b). We also examined the interaction between HRas and wild-type BRaf at a single prey concentration of 1 nM. The measured k_{on} value was higher than those of the $BRaf^{V600E}$ mutant and CRaf (Figure 2a, 0.39 ± 0.02 μM^{-1} s^{-1}), but the measured k_{off} value of 0.62 ± 0.02 s^{-1} was very similar to that of $BRaf^{V600E}$ (Figure 2b). These kinetic rates gave apparent K_d values of 3.6 ± 0.4, 2.3 ± 0.2, and 1.6 ± 0.1 μM for the HRas-CRaf, HRas-$BRaf^{V600E}$, and HRas-BRaf complexes, respectively (Figure 2c). Taken together, our results corroborate the possibility that a PPI can be characterized using a prey protein concentration 4 orders of magnitude lower than the K_d value.

To explore the upper limit of K_d accessible with the current approach, we attempted to measure interaction of a dominant negative (DN) form of HRas ($HRas_{DN}$, S17N mutant) with full-length Rafs, which is known to be extremely weak. To monitor these interactions, we immobilized the $HRas_{DN}$ proteins at a high density of 1200 baits per μm^2 and monitored PPIs using 10 nM CRaf and 9.4 nM $BRaf^{V600E}$, respectively (Figure 2d). The k_{on} values were 0.67 ± 0.06 and 0.33 ± 0.01 mM^{-1} s^{-1} for the $HRas_{DN}$-CRaf and $HRas_{DN}$-$BRaf^{V600E}$ interactions, respectively, more than 2 orders of magnitude smaller than those measured with the $HRas_{CA}$ (Figure 2e). However, the k_{off} values were determined to be 0.88 ± 0.02 s^{-1} and 0.51 ± 0.04 s^{-1} for CRaf and $BRaf^{V600E}$, respectively, which were almost identical to those measured with the $HRas_{CA}$ proteins. Because of the extremely low k_{on}, the resulting K_d values were 1.31 ± 0.12 and 1.56 ± 0.13 mM for the CRaf- and $BRaf^{V600E}$-$HRas_{DN}$ complexes, respectively (Figure 2e).

Finally, to see whether our approach can be applied to other types of PPI beyond the Ras-Raf interactions, we sought to measure the interaction between Ras and p110, which is the catalytic subunit of PI3K. The p110 subunit, also containing RBD, is found to interact with Ras, suggesting a molecular mechanism of signaling crosstalk between the MAPK and PI3K pathways. However, the interaction kinetics has not been characterized so far.

We expressed three different isoforms, α, β, and δ isoforms, of p110 in separate pools of HEK293 cells and measured their interactions with the CA and DN forms of HRas. Only the α isoform of p110 showed interaction with the CA form of HRas (Figure 3a). This observation indicates a high level of isoform specificity in the Ras-PI3K interaction.

To determine the kinetic rates of the Ras-p110α interaction, we measured this PPI at different prey protein concentrations

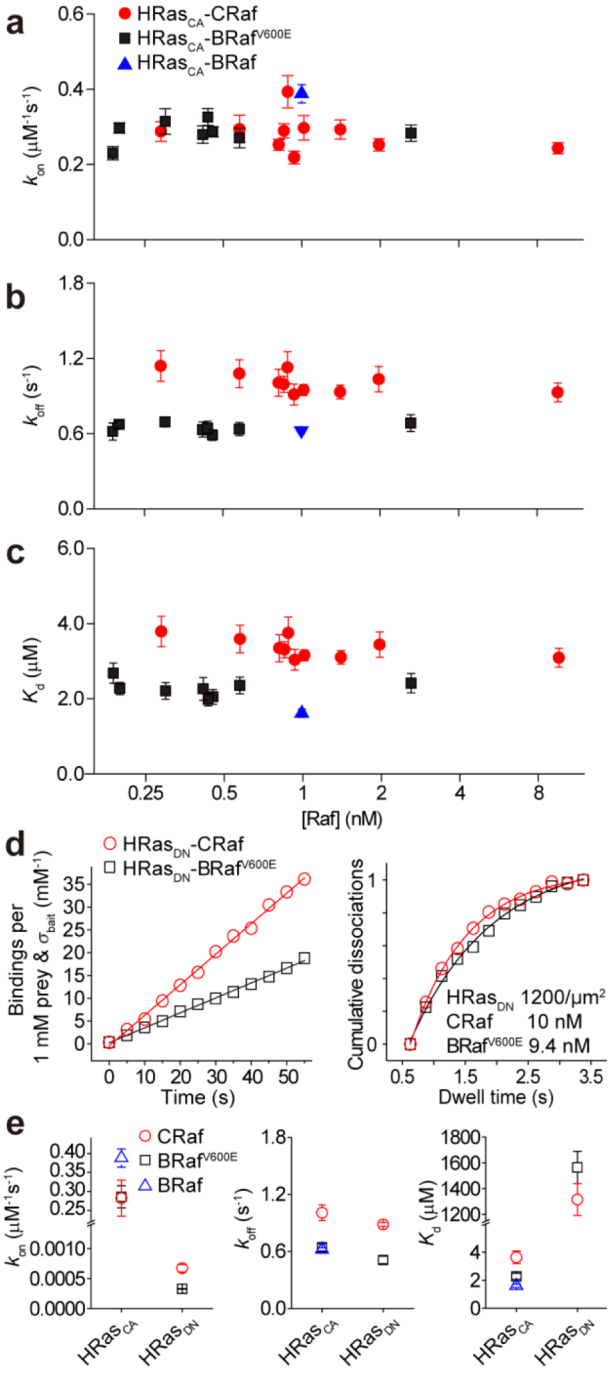

Figure 2. (a) k_{on}, (b) k_{off}, and (c) K_d of the HRas-CRaf, HRas-$BRaf^{V600E}$ and HRas-BRaf interactions. (d) Binding and unbinding kinetics of $HRas_{DN}$-CRaf and $HRas_{DN}$-$BRaf^{V600E}$. (e) Comparison of k_{on}, k_{off}, and K_d between $HRas_{CA}$ and $HRas_{DN}$ interactions.

(1.0−8.0 nM), which were combined with HRas densities of 22.2−43.3 per μm^2. The measured kinetic rates showed consistent values in the concentration range we studied, which gave k_{on} of 0.15 ± 0.01 μM^{-1} s^{-1} and k_{off} of 0.28 ± 0.01 s^{-1}. These kinetic rates were combined to yield a K_d value of 1.9 ± 0.1 μM for the HRas-p110α interaction (Figures 3b−d and SI-15).

Our work provides a general method to characterize PPIs using a prey protein concentration 3−4 orders of magnitude lower than the K_d value. We determined micromolar K_d values with prey concentrations of <1 nM. We were even able to

DOI: 10.1021/jacs.6b09542
J. Am. Chem. Soc. 2016, 138, 14238−14241

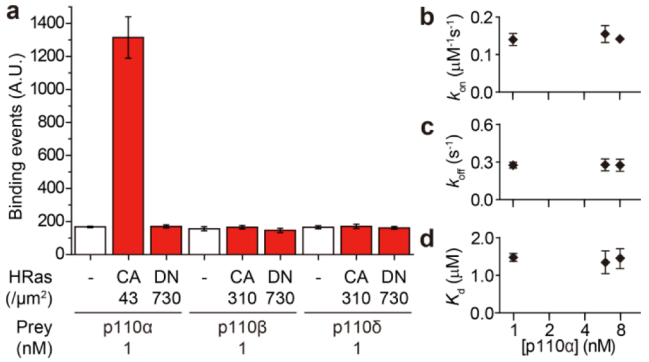

Figure 3. (a) Comparison of observed binding events for depicted reaction conditions. (b) k_{on}, (c) k_{off}, and (d) K_d of the HRas-p110α interaction.

determine a K_d value in a millimolar range using a prey concentration of 10 nM (for inactive Ras and full-length Rafs). Given that the concentration barrier is around tens of nM for the TIR fluorescence microscopy, the approach described here would enable determination of millimolar K_d values without major modifications to conventional single-molecule microscopy.

We note that employment of single-molecule co-IP analysis was important, as it provided a strategy to observe the interactions of large mammalian proteins such as full-length Rafs and different isoforms of p110. Large-scale expression and purification were not readily possible for these proteins, which may explain why in vitro characterization of the full-length Rafs and p110 isoforms has been difficult to carry out. The single-molecule co-IP analysis provides a strategy to observe dynamics of the target proteins as long as their genes can be tagged with fluorescent proteins and transiently expressed in mammalian cells.

In our experiments, we lowered prey protein concentrations in a proportionate way as we increased the surface density of baits. Thus, we did not see any rebinding of prey proteins to the crowded baits in the three different types of PPIs we examined. In physiological conditions, where many membrane-associated proteins exist at a high surface density, we presume that the rebinding effect may play a role,[18] which would render the effective binding kinetic rate higher than the values observed in this work.

Finally, the kinetic rates of weak PPIs determined in this study may provide a glimpse of the dynamic regime exploited by the cell signaling circuit. The PPIs with micromolar K_d values exhibited higher association kinetic rates (k_{on}) than anticipated, all at around 10^6 M^{-1} s^{-1}, which were similar to that of typical antibody–antigen binding. This high k_{on} value is balanced by the high dissociation rates (k_{off}), which concentrated around 1 s^{-1}. Thus, at least in this case of the PPI network built around Ras, the cell signaling circuit takes advantage of turnover on a second time scale and seems to modulate the association rate in order to regulate its signal flows.[22]

■ ASSOCIATED CONTENT

Supporting Information

The Supporting Information is available free of charge on the ACS Publications website at DOI: 10.1021/jacs.6b09542.

Experimental details and data (PDF)

■ AUTHOR INFORMATION

Corresponding Author

*tyyoon@yonsei.ac.kr

Notes

The authors declare no competing financial interest.

■ ACKNOWLEDGMENTS

This work was supported by the National Creative Research Initiative Program (Center for Single-Molecule Systems Biology to T.-Y.Y., NRF-2011-0018352) and the A3 Foresight Program (to T.-Y.Y., 2013K2A2A6000534, FY2013) through the National Research Foundation of Korea (NRF) funded by the Korean government. This work was also supported by the Institute for Basic Science (IBS; IBS-R0216-D1).

■ REFERENCES

(1) Klug, A. *Annu. Rev. Biochem.* **2010**, *79*, 213.
(2) Sternberg, S. H.; Redding, S.; Jinek, M.; Greene, E. C.; Doudna, J. a. *Nature* **2014**, *507* (7490), 62–67.
(3) Schreiber, G.; Haran, G.; Zhou, H. X. *Chem. Rev.* **2009**, *109* (3), 839–860.
(4) Perkins, J. R.; Diboun, I.; Dessailly, B. H.; Lees, J. G.; Orengo, C. *Structure* **2010**, *18* (10), 1233–1243.
(5) Joo, C.; Balci, H.; Ishitsuka, Y.; Buranachai, C.; Ha, T. *Annu. Rev. Biochem.* **2008**, *77*, 51–76.
(6) van Oijen, A. M. *Curr. Opin. Biotechnol.* **2011**, *22* (1), 75–80.
(7) Holzmeister, P.; Acuna, G. P.; Grohmann, D.; Tinnefeld, P. *Chem. Soc. Rev.* **2014**, *43* (4), 1014–1028.
(8) Mertz, J.; Xu, C.; Webb, W. W. *Opt. Lett.* **1995**, *20* (24), 2532.
(9) Diaspro, A.; Chirico, G.; Collini, M. *Q. Rev. Biophys.* **2005**, *38* (2), 97–166.
(10) Betzig, E.; Chichester, R. J. *Science* **1993**, *262* (5138), 1422–1425.
(11) de Lange, F.; Cambi, a; Huijbens, R.; de Bakker, B.; Rensen, W.; Garcia-Parajo, M.; van Hulst, N.; Figdor, C. G. *J. Cell Sci.* **2001**, *114*, 4153–4160.
(12) Levene, M. J.; Korlach, J.; Turner, S. W.; Foquet, M.; Craighead, H. G.; Webb, W. W. *Science* **2003**, *299* (5607), 682–686.
(13) Miyake, T.; Tanii, T.; Sonobe, H.; Akahori, R.; Shimamoto, N.; Ueno, T.; Funatsu, T.; Ohdomari, I. *Anal. Chem.* **2008**, *80* (15), 6018–6022.
(14) Uemura, S.; Aitken, C. E.; Korlach, J.; Flusberg, B. a; Turner, S. W.; Puglisi, J. D. *Nature* **2010**, *464* (7291), 1012–1017.
(15) Loveland, A. B.; Habuchi, S.; Walter, J. C.; van Oijen, A. M. *Nat. Methods* **2012**, *9* (10), 987–992.
(16) Sydor, J. R.; Engelhard, M.; Wittinghofer, A.; Goody, R. S.; Herrmann, C. *Biochemistry* **1998**, *37* (40), 14292–14299.
(17) Kiel, C.; Filchtinski, D.; Spoerner, M.; Schreiber, G.; Kalbitzer, H. R.; Herrmann, C. *J. Biol. Chem.* **2009**, *284* (46), 31893–31902.
(18) Lee, H.-W.; Kyung, T.; Yoo, J.; Kim, T.; Chung, C.; Ryu, J. Y.; Lee, H.; Park, K.; Lee, S.; Jones, W. D.; Lim, D.-S.; Hyeon, C.; Heo, W.; Do Heo, W.; Yoon, T.-Y. *Nat. Commun.* **2013**, *4*, 1505.
(19) Lee, H.-W.; Ryu, J. Y.; Yoo, J.; Choi, B.; Kim, K.; Yoon, T.-Y. *Nat. Protoc.* **2013**, *8* (10), 2045–2060.
(20) Jain, A.; Liu, R.; Ramani, B.; Arauz, E.; Ishitsuka, Y.; Ragunathan, K.; Park, J.; Chen, J.; Xiang, Y. K.; Ha, T. *Nature* **2011**, *473* (7348), 484–488.
(21) Stephen, A. G.; Esposito, D.; Bagni, R. G.; McCormick, F. *Cancer Cell* **2014**, *25* (3), 272–281.
(22) Schreiber, G. *Curr. Opin. Struct. Biol.* **2002**, *12* (1), 41–47.

DOI: 10.1021/jacs.6b09542
J. Am. Chem. Soc. 2016, 138, 14238–14241